Desalination and Water Treatment
www.deswater.com
doi: 10.5004/dwt.2021.27183

224 (2021) 407–420
June

Zeolite imidazolate framework-11 for efficient removal of Bromocresol Green in aqueous solution, isotherm kinetics, and thermodynamic studies

Rachid Lamari[a,*], Bénamar Benotmane[a], Samira Mezali[b]

[a]*URMPE, M'Hamed Bougara University, Boumerdes 35000, Algeria, Tel. +213 662044327/213 659010318; emails: r.lamari@univ-boumerdes.dz (R. Lamari), b.benotmane@univ-boumerdes.dz (B. Benotmane)*
[b]*Faculty of Sciences, Chemical Department, M'Hamed Bougara University, Boumerdes 35000, Algeria, Tel. +213 553726873; email: s.mezali@univ-boumerdes.dz*

Received 16 May 2020; Accepted 19 February 2021

ABSTRACT

In this study, zeolitic imidazolate framework (ZIF-11) type was synthesized by stirring method and used for the removal of Bromocresol Green (BCG) from aqueous solutions. For this purpose, the ZIF-11 particles were analysed by X-ray diffraction, scanning electron microscope, Fourier-transform infrared spectroscopy, thermogravimetric analysis, and differential scanning calorimetry. In batch experiments, the effective BCG adsorption parameters onto ZIF-11 particles were examined. Based on the characterization results, the synthesized ZIF-11 showed a highly porous, irregular, and inhomogeneous shapes and crystals with varying sizes as well as high thermal stability. The adsorption results indicated that the highest BCG removal (89%) was obtained when the solution pH, the stirring speed, the contact time, and the temperature were adjusted to 6.8, 400 rpm, 30 min, and 298 K, respectively. The adsorption data fitted well to Langmuir and Temkin models with maximum adsorption capacity of 150 mg/g. The adsorption kinetics was compatible with the pseudo-second-order and the intraparticle diffusion models. Indeed, BCG molecules instantaneously adsorbed on the external surface of ZIF-11 particles and gradually diffused within theirs pores. The negative value of free energy change and positive values of enthalpy and entropy changes showed the feasibility, randomness, and endothermicity of the BCG adsorption process, which was found to be physicochemical based.

Keywords: Bromocresol Green; ZIF-11; Isotherm; Kinetics; Thermodynamic

1. Introduction

Wastewater, mainly discharged from the textile, tannery, printing, and food industries contain dyes, which are the source of severe pollution because of their non-biodegradability. The widely used basic, acid, reactive, and disperse dyes affect the nature of water by reducing photosynthetic reactions. Moreover, some dyes are toxic and even carcinogenic [1]. These contaminants have to be removed from the industrial effluents, which are currently considered as one of the main environmental concerns. It has been reported that the frequently used techniques for the treatment of wastewater included adsorption, coagulation–flocculation, and oxidation–ozonation [2–4]. Most commonly, the adsorption process is the cost-effective operation and is widely employed for the removal of different pollutant substances: arsenic, chromium, and dyes [5–7].

As one of the most common dyes, Bromocresol Green (BCG) is widely used as raw material in a sol–gel matrix, textile, dental materials, leather, paper, printing, detergents, and plastic [8]. However, it is a part of dye found as a pollutant in the environment affecting aqua life, human health

* Corresponding author.

through consumption of water and food. BCG: (2,6-dibromo-4-[7-(3,5-dibromo-4-hydroxy-2-methyl-phenyl)-9,9-dioxo-8-oxa 96 thiabicyclo [4.3.0]nona-1,3,5-trien-7-yl]-3-methyl-phenol) (Fig. 1a) is a triphenylmethane generally used as a pH indicator, DNA tracer, depends on pH value and has a different color [9,10]. In an aqueous solution, BCG dissociates to monoanionic form (pK_a of 4.8) and gets yellow color and at higher pH, it changes to dianionic form and gets blue color [10]. As a result, at low solution pH the positively charged adsorbent surface attract BCG molecules and repel them at high pH. This was observed for the removal of BCG from water by means of solvent sublation [11] or by adsorption onto different adsorbents as activated carbon [9,12], chitosan polymethacrylate composites [13], electrospun scaffolds [14], and *Ziziphus nummularia* [10]. However, efficient adsorption depends more on the adsorbent capacity than on operating conditions for which the solution's pH value is important. In that respect, zeolitic imidazolate frameworks (ZIFs) as well as metal organic frameworks, which are highly porous materials with high chemical and thermal stability, are useful in the adsorption of organic dye molecules because of their modifiable porous structures [15–19]. Mainly, ZIF-67 and ZIF-8 were used to conduct efficient removal of several hazardous pollutants such as Cr(VI) [20], phenol [21], anionic organic dyes [22–25], in which the main adsorption mechanism included electrostatic interactions, ion exchange, and π–π interactions. However, it was reported that the small aperture size of some ZIFs limits the diffusion of dye molecules into their internal porous structure, while on the external surface, many active adsorption sites allow dye molecules to be attracted to specific functional groups [26].

In this paper, the feasibility of ZIF-11 (Fig. 1b) as adsorbent was investigated for the removal of BCG from aqueous solutions. To this purpose, ZIF-11 particles were synthesized by stirring method and characterized by different known experimental techniques. For BCG batch adsorption onto ZIF-11, the operational parameters, isotherms, kinetics, and thermodynamic parameters were assessed.

2. Materials and methods

2.1. Instruments

During experiments, the BCG concentration was evaluated at 412 nm (using UV-Visible spectrophotometer model PG INSTRUMENTS T60) based on respective linear calibration curve over desired understudy concentration range. The pH of sample solution was adjusted by addition of HCl or NaOH using a pH meter model-8603 Seven Easy, METTLER TOLEDO, Switzerland.

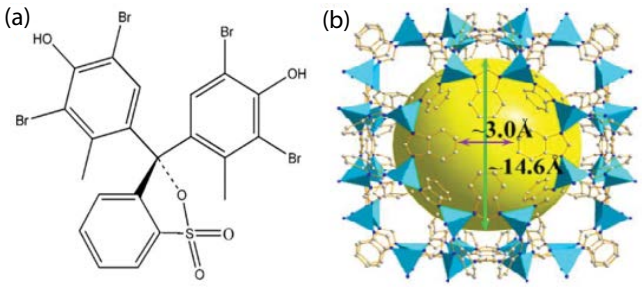

Fig. 1. (a) Bromocresol Green structure. (b) Schemes for the crystal structure of ZIF-11. Both sided arrows indicate the pore diameter and aperture [29].

2.2. Chemicals

Zinc acetate dihydrate (ZnAc, $Zn(CH_3)_2{\cdot}2H_2O$, >99.99%, E. MERCK, Germany), benzimidazole (bIM) ($C_7H_6N_2$, 98%), and methanol (CH_3OH, 99.8%) were purchased from Sigma–Aldrich (India). Ammonium hydroxide (NH_3, 25% aqueous solution) was purchased from BIOCHEM Chemopharma, and toluene ($C_6H_5CH_3$, 98.8%) was purchased from Panreac. NaOH and HCl were purchased from Sigma–Aldrich (India). BCG was purchased from National Pharmaceutical Group Chemical Reagent Co., Ltd. (China) and used without further purification. Deionized water (DI) with a conductivity of 6×10^{-2} μS/cm was used in the preparation of all samples and standards. The chemicals were of analytical grade and were used as received without further purification.

2.3. Preparation of the adsorbents

ZIF-11 crystal was synthesized in a purely aqueous system by the stirring method as reported in the literature [27–29]. Synthesis was performed at room temperature (20°C ± 2°C), with gentle stirring (200 rpm) in a vial (100 mL) for 2 h. A 2.506 mmol of zinc acetate dihydrate was dissolved in 524.344 mmol of methanol and 141.089 mmol of toluene. The two solutions were stirred until the total dissolution of the solutes (bIM and ZnAc), and were mixed under stirring. The resulting of ZIF-11 (precipitation of a white solid) was collected by centrifugation, washed with methanol and dried in oven at 120°C overnight to evaporate the trapped toluene and methanol (yield: 0.1422 g, 89.70%).

2.4. Experimental procedure

Adsorption experiments were carried out in batches. For that purpose, known amounts of ZIF-11 were added to the accurately prepared BCG solutions. The mixtures were placed in a stirring incubator (IKA® RCT basic safety control) until the adsorption equilibrium was achieved. By filtration through a 0.45 μm membrane, the charged particles of ZIF-11 were separated from the BCG solutions, whose concentrations were measured by UV-Visible spectrophotometer. The acquired values were used for the determination of the adsorption parameters.

The amount of adsorbed BCG at equilibrium Q_e (mg/g) shortly referred as adsorption amount or adsorption capacity was determined by the following equation:

$$Q_e = \frac{\left(C_0 - C_e\right)}{m} V \tag{1}$$

where C_0 and C_e (mg/L) are the initial and equilibrium BCG concentrations, V (L) is the volume of the solution, and m (g) is the mass of the adsorbent (ZIF-11).

The BCG removal efficiency R_E is a measure of the adsorption performance. It can be calculated as follows:

$$R_E(\%) = \frac{(C_0 - C_e)}{C_0} \times 100 \quad (2)$$

2.5. Validity of adsorption isotherm and kinetic models

Usually, in the adsorption equilibrium studies, isotherm and kinetic models are fitted to experimental data in order to predict the mechanisms of various adsorption systems. The models are mainly non-linear; however, they can be linearized for ease of use and exploitation. For optimum adsorption data analysis the best fitting models are required. This requires the use of either linear regression or non-linear regression analysis using error functions, of which the statistics are described below.

The sum of squared errors (SSE) is the measure of the variance of the measured data from the true mean of the data. The least square technique for estimating regression coefficients minimizes this statistic. Eq. (3) gives SSE values:

$$\text{SSE} = \sum_{i=1}^{N}\left[\left(Q_{e,\text{exp}} - Q_{e,\text{cal}}\right)^2\right]_i \quad (3)$$

The root mean square error (RMSE) is a standard way to measure the error (deviation) of a model in predicting quantitative data. A smaller RMSE means that the model fits the data well. Formally, it is defined as follows:

$$\text{RMSE} = \sqrt{\frac{\sum_{i=1}^{N}\left[\left(Q_{e,\text{exp}} - Q_{e,\text{cal}}\right)^2\right]_i}{N}} \quad (4)$$

Hybrid fractional error function (HYBRID) (Eq. (5)) is an error function developed to improve the adjustment of the SSE at low concentrations divided by the experimental value of the adsorbed BCG and includes the degrees of freedom of the system (adsorbate/adsorbent).

$$\text{HYBRID} = \frac{100}{N-p}\sum_{i=1}^{N}\left[\frac{\left(Q_{e,\text{exp}} - Q_{e,\text{cal}}\right)^2}{Q_{e,\text{exp}}}\right]_i \quad (5)$$

The chi-square statistic (χ^2), which is used as a criterion for the quality of fitting, is given by Eq. (6):

$$\chi^2 = \sum_{i=1}^{N}\frac{\left(Q_{\text{exp}} - Q_{\text{cal}}\right)^2}{Q_{\text{exp}}} \quad (6)$$

The coefficient of determination represents the variance about the mean; it is used to analyze the fitting degrees of isotherm and kinetic models with experimental data. The coefficient of determination R^2 is defined by the following equation:

$$R^2 = 1 - \frac{\sum_{i=1}^{N}\left[\left(Q_{e,\text{exp}} - Q_{e,\text{cal}}\right)^2\right]_i}{\sum_{i=1}^{N}\left[\left(Q_{e,\text{exp}} - \overline{Q_{e,\text{exp}}}\right)^2\right]_i} \quad (7)$$

In these equations, $Q_{e,\text{exp}}$ indicates the experimental (measured) values of the amount of adsorbed BCG at equilibrium and $\overline{Q_{e,\text{exp}}}$ is its average value, whereas $Q_{e,\text{cal}}$ is its calculated value, which is obtained from the fitted isotherm model. N is the number of tests and p is the number of parameters in the isotherm equation.

2.6. Characterization techniques

2.6.1. X-ray diffraction

The crystallographic structure of ZIF-11 synthesized was analyzed using a PANalytical X-Pert Pro, Empyrean Cu LFF HR (9430 033 7310x) DK417340 with CuKα radiation at a scan rate of 2θ = 0.001 from 4.99 to 90 and λ = 1.54 Å. The accelerating voltage and applied current were 45 kV and 40 mA, respectively.

2.6.2. Scanning electron microscope

The prepared ZIF-11 microstructure was observed using scanning electron microscope (SEM; QUANTA 650). The material was deposited on an adhesive and conductive observation medium, and then was metalized with argon plasma. The observation was carried out under vacuum at an accelerating voltage of 5 kV.

2.6.3. Fourier-transform infrared spectroscopy

The Fourier-transform infrared (FTIR) spectrophotometer was used to identify the characteristic functional groups in the adsorption onto ZIF-11. For that, 5 mg of ZIF-11 was mixed and pressed under a high pressure (4,500 psi) with dry spectroscopic KBr to form thin disc. Then, the IR spectrum was plotted with a Nicolet™ iS™ 10 spectrometer between 400 and 4,000 cm^{-1}.

2.6.4. Thermogravimetric analysis and differential scanning calorimetry

The thermogravimetric analysis (TGA) and differential scanning calorimetry (DSC) of the ZIF-11 particles were carried out in a N_2 atmosphere at a scan speed of 10 K/min from 50°C to 700°C on a NETZSCH STA 409PC/PG.

3. Results and discussion

3.1. Characterization of ZIF-11 synthesized

3.1.1. X-ray diffraction

The powder X-ray diffraction (XRD) patterns for the ZIF-11 samples synthesized by stirring method before adsorption (a), after BCG adsorption at 25°C (b), and simulated ZIF-11 (c) [13] are shown in Fig. 2. In Fig. 2c, the diffraction peaks at 2θ = 3.07°, 4.34°, 6.14°, 7.52°, 8.69°, 12.30°, 13.76°, 15.70°, 17.42°, and 18.50° correspond to the planes (100), (110), (200), (211), (220), (400), (420), (510), (440), and (600), respectively [19]. Compared to the simulated ZIF-11, the synthesized samples showed overall similarity in XRD peaks but also displayed a slight peak shift towards high two-theta angles at 2θ = 6.21° and

7.62° corresponding to the planes (200) and (211), respectively. This may be indicative of the decrease in interplanar spacing, due to framework flexibility, a typical feature of several microporous crystals, including ZIFs [24,25].

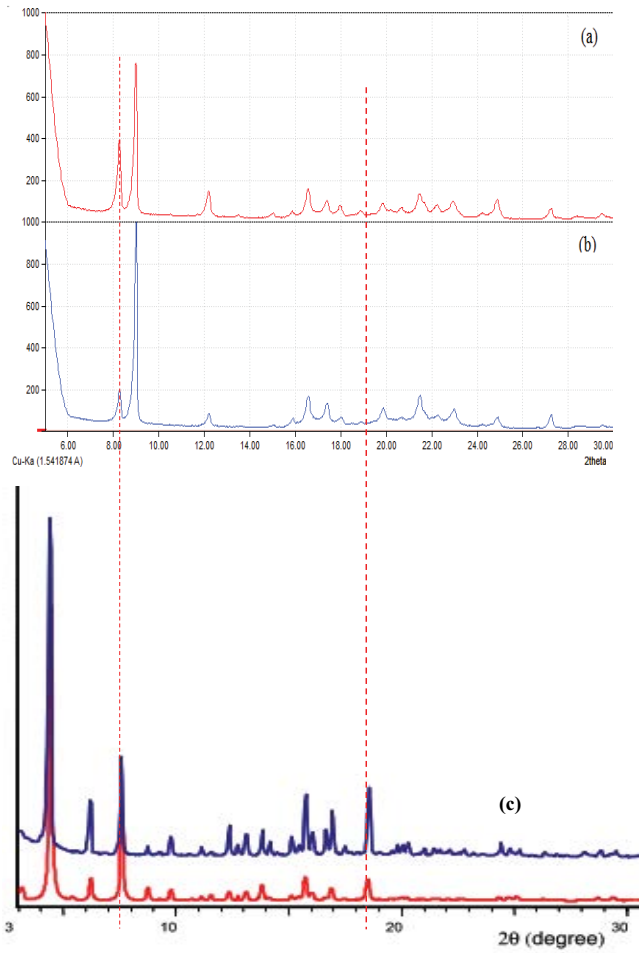

Fig. 2. Powder XRD patterns of the measured ZIF-11 samples ((a) before adsorption tests and (b) after adsorption tests) achieved several times at 25°C and simulated ZIF-11(*) (c).

Furthermore, the intensity of the main peaks corresponding to the (200) and (211) planes, was higher for the synthesised samples. This suggests a higher degree of crystallinity with local structural disorder due to variable and irregular shapes of the synthesized samples compared to the simulated pattern. It can also be noticed that there was no shift in the peak in the XRD result of the synthesized samples before and after adsorption (Figs. 2a and b).

3.1.2. Scanning electron microscope analysis of ZIF-11 particle

The surface morphology of ZIF-11 particles as illustrated in Fig. 3 was assimilated by SEM. It was clear that the ZIF-11 exhibited a highly porous, irregular, and inhomogeneous shapes and variable size. From the results obtained, it is concluded that ZIF-11 can successfully be synthesized by stirring method using anhydrous zinc chloride and bIM in a binary solvent mixture (methanol and toluene) at room temperature (≈25°C).

3.1.3. Fourier-transform infrared spectroscopy

To ascertain the main functional groups of the synthesised samples of ZIF-11, FTIR spectrum was utilized. As shown in Fig. 4, all frequencies associated with the bonds contained within the bIM ring were available. Weak peaks at 3,088 and 3,032 cm^{-1} indicated stretching vibrations of =C–H, while more intense peaks at 1,606 and 1,547 cm^{-1} were attributed to C=C stretching. The C–C stretching occurred at 1,465 cm^{-1} and bonds at 1,281 and 1,243 cm^{-1}. The bands occurring at around 530–400 cm^{-1} were fingerprints of ZnO. In particular, the band at 427 cm^{-1} corresponding to Zn–N stretching indicated the successful bond formation between zinc ions and the bIM organic linker. In this context, we can assume that the reaction of Zn^{2+} and bIM in ZIF-11 crystals occurred. These results are slightly similar to those obtained by other authors [19,29–31]. The bIM ring presents two regions [32]: one is nucleophilic (set of positive charges) located on the C–H bonds of the benzyl ring, the other is electrophilic (set of negative charges) located around the imidazole group. These charge distributions are responsible

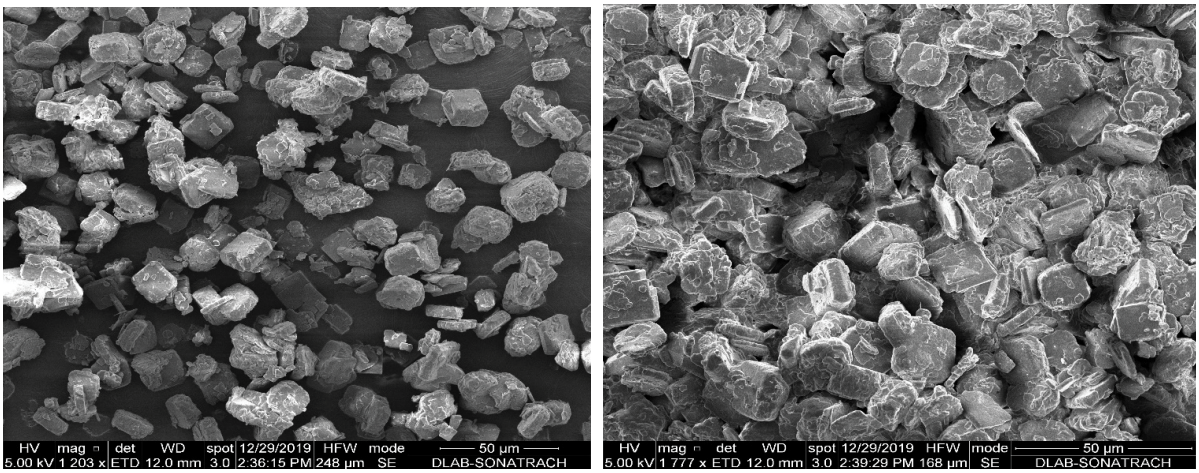

Fig. 3. Scanning electron microscope pictures of ZIF-11 particles.

on molecular interactions between electron acceptors (benzyl ring of the bIM) and the electron donors (Zn^{2+}). In addition, electron donors of the six-membered ring of the bIM are available for interactions with other molecules in adsorption for instance.

3.1.4. Thermogravimetric and differential scanning calorimetry analysis

The thermogravimetric (TG) and DSC analysis of ZIF-11 were performed to study the thermal stability of ZIF-11 particles (Fig. 5). As shown in the TG curve between 150°C and 220°C, the first weight-loss of the sample was very small (about 2%), relating to the removal of guest molecules like toluene withheld in the particle cages. The long gradual plateau in the TGA up to 540°C indicated that the skeleton of ZIF-11 has high thermal stability. The second weight-loss of 6% occurred from 480°C to 540°C indicating the framework collapse, which was caused by the decomposition process of the organic ligands that are bIM. The weight-loss process was complete (71%) at 640°C and the residue (29%) was zinc oxide (ZnO). The DSC curve exhibited two exothermic peaks at 558°C and 643°C corresponding to a skeleton decomposition in two stages. The first is related to irregularly shaped and small particles, the second to more regular crystals, both of which are part of the ZIF-11 sample (Fig. 3). These results are in agreement with those observed by [19,29,31].

3.2. Influence of process parameters

3.2.1. Effect of the solution pH

The solution pH has an important influence on the surface electrical properties of the ZIF-11 particles and consequently on the adsorption of BCG dye. The effect of solution pH on the adsorption of BCG dye was investigated in the range of pH values 2.0–12. For this purpose, the point of zero charge (pH_{PZC}) for ZIF-11 was estimated by a mass titration method [33]. The graph of final pH versus initial pH was used to determine the point at which the initial pH and final pH values were equal (Fig. 6). The

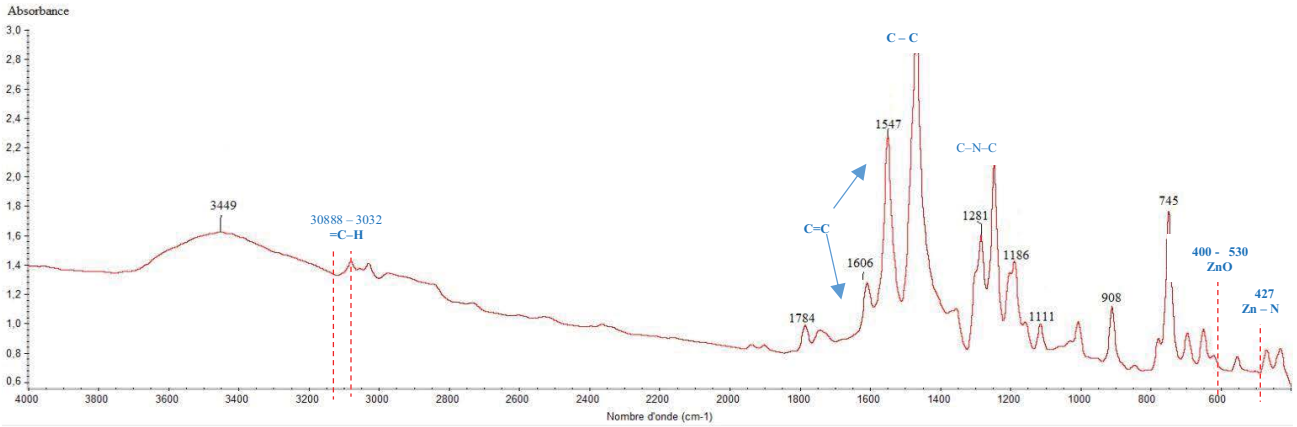

Fig. 4. Fourier-transform infrared spectroscopy spectrum of prepared ZIF-11 crystals.

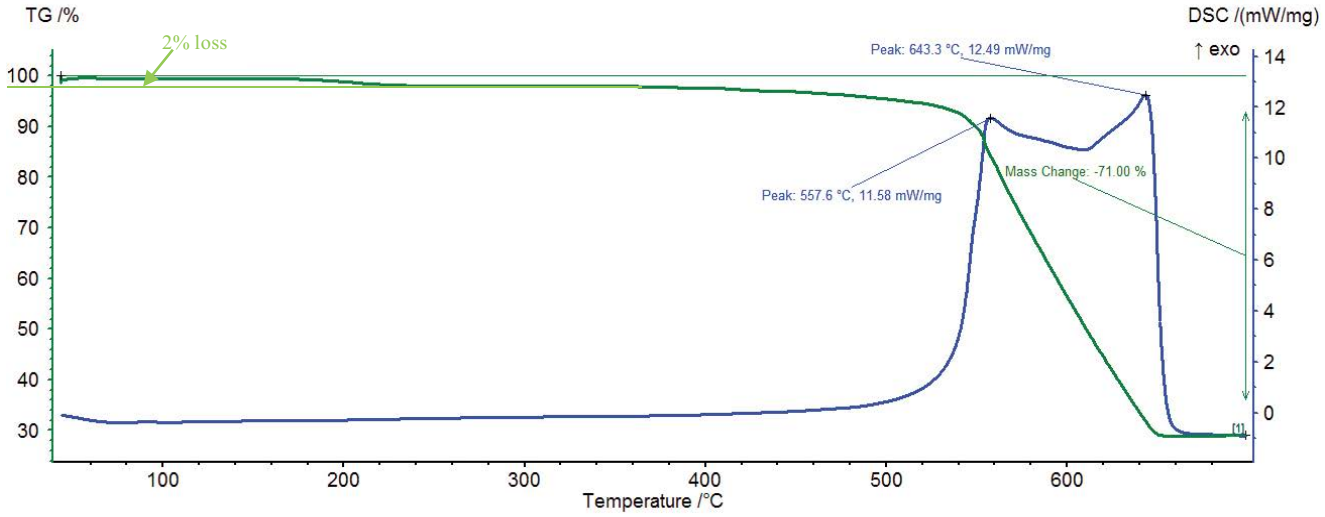

Fig. 5. TGA/DSC of prepared ZIF-11 crystals.

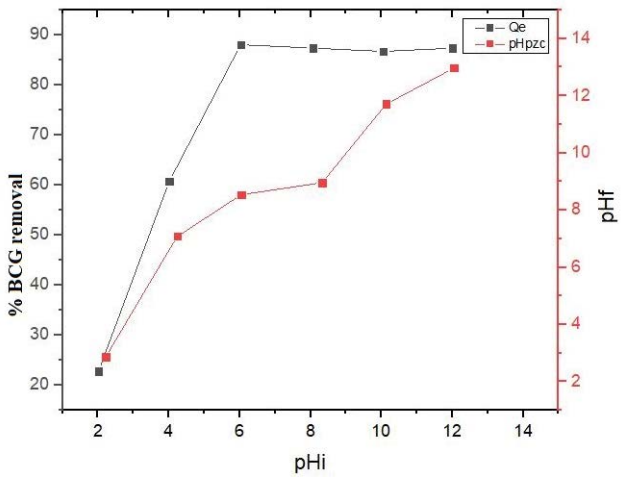

Fig. 6. Effect of pH on the adsorption of BCG onto ZIF-11.

value of pH_{PZC} corresponded to 8.1 indicating slight basicity of the particles surface. At lower pH, the ZIF-11 surface is positively charged and vice versa. In most cases, ZIF-11 had a positive surface charge at a wide pH range (from 2.0 to 8.0) and could adsorb anionic BCG dyes through electrostatic interactions forming ion-pair complexes ($[ZIF]^+[BCG]^-$). Furthermore, ZIFs have a bifunctional property with dual Lewis acidic (Zn atom) and basic sites (–NH groups of the imidazolate linkers) [34,35]. This bifunctional property could allow ZIF-11 crystals to be a potential adsorbent for BCG molecules, as they can interact via special functional groups such as SO_3 or OH. These assumptions are supported by BCG adsorption results as a function of pH solution, which indicated an increase in adsorption capacity with an increase in pH up to 6.8 (Fig. 6). Above this value, the adsorption capacity remained almost constant due most likely to repulsive forces between ZIF-11 and BCG surfaces. Therefore, pH = 6.8 was selected as an optimum parameter.

3.2.2. *Influence of stirring speed*

The stirring is essentially needed to maximize the interactions between BCG molecules and adsorption sites of ZIF-11 particles in the solution. The effect of stirring speed over the range (100–600 rpm using a mechanical agitator and magnetic stirrer) on the BCG adsorption capacity onto ZIF-11 was investigated and the results are shown in Fig. 7. It is found that the BCG adsorption capacity increased with an increase in stirring speed from 100 to 400 rpm and then it remained approximately constant with further increasing. The water-insoluble BCG molecules, when strongly agitated, disperse in the solution and diffuse towards the particles' surface to be adsorbed. This effect remained constant above 400 rpm, which is the optimal level to be selected for further steps of this study.

3.2.3. *Effect of initial concentration*

BCG initial concentration, contact time, and the solution temperature are important for the assessment of the settings of the batch adsorption process. The effect of the initial concentration of BCG on the adsorption process was investigated for concentrations ranging from 20 to 300 mg/L and results are summarized in Fig. 8. It can be seen that the removal efficiency decreases rapidly as the initial BCG concentration increases. At lower concentrations, a sufficient number of adsorption sites are available to ensure a favorable adsorption of BCG molecules, and the inverse occurs at higher concentrations [36]. Efficient removal, in this case, is achieved with low initial concentration solutions (up to 100 mg/L), which in practice meets the environmental requirements.

3.2.4. *Effect of contact time*

The effect of contact time on the amount of BCG dye adsorbed by ZIF-11 was investigated at four initial BCG dye concentrations: 20, 40, 60, and 80 mg/L. It can be seen that the adsorption process took place in two stages (Fig. 9). The first stage was rapid wherein the first 10 min

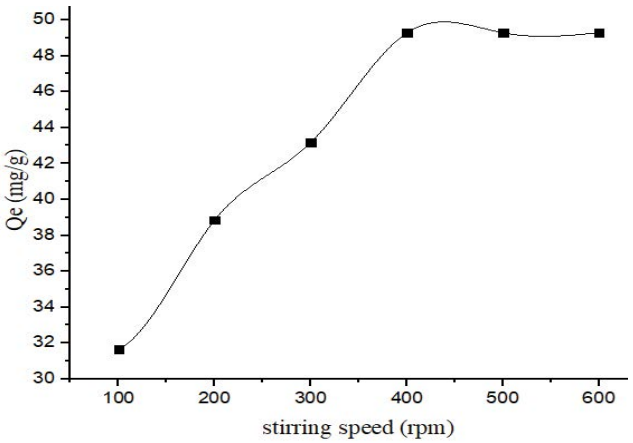

Fig. 7. Effect of stirring speed on the adsorption of BCG onto ZIF-11.

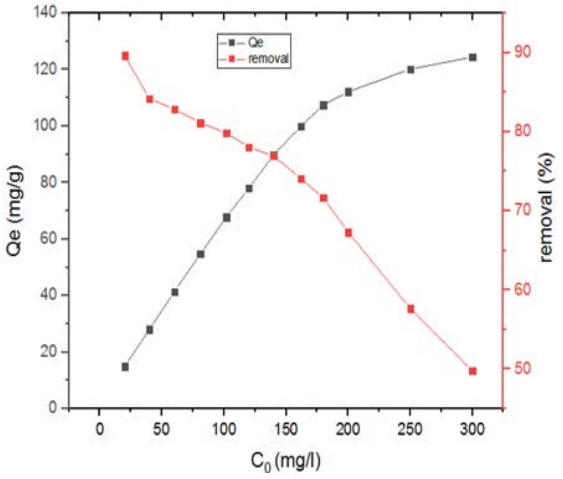

Fig. 8. Effect of initial concentration on the adsorption of BCG onto ZIF-11.

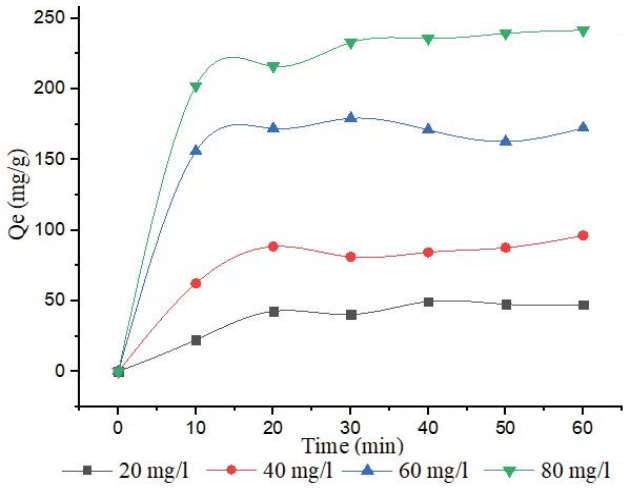

Fig. 9. Effect of contact time on the adsorption of BCG onto ZIF-11 at different initial BCG concentrations.

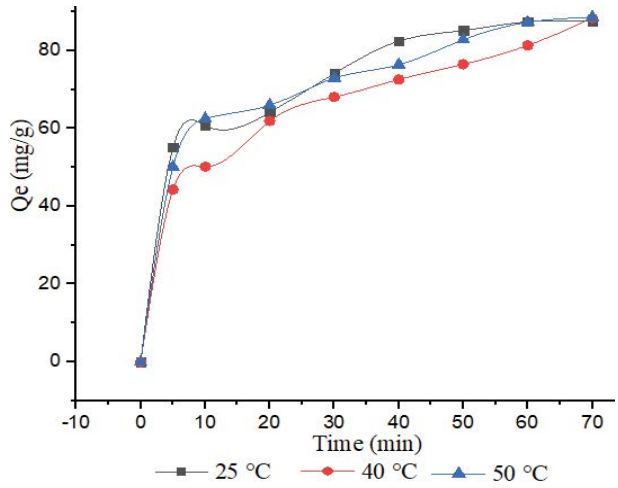

Fig. 10. Effect of temperature on the adsorption of BCG onto ZIF-11.

the removal efficiency was 75% of BCG from a solution of 80 mg/L initial concentration. This is due to the large gradient between the number of vacant sites available on the ZIF-11 surface and the number of BCG molecules in solution resulting in a high frequency of BCG/ZIF-11 collisions [25]. The second stage represented a slower progressive adsorption process up to 30 min contact time indicating saturation of adsorption sites. For BCG solutions with initial concentrations lower than 80 mg/L, the previously described behavior remained similar and the removal efficiency increased from 81% to 89% for a contact time of 30 min. Obviously, at lower concentrations, there are enough adsorption sites available to adsorb BCG molecules, and the inverse occurs at higher concentrations. Thus, for investigating the adsorption equilibrium of BCG on ZIF-11, the optimal contact time was chosen as 30 min.

3.2.5. Effect of temperature

The effect of temperature on the adsorption process was investigated at different contact times ranging from 10 to 70 min and the results are summarized in Fig. 10. The adsorption process followed the same stages as described above (subsection 3.2.4), with a pronounced adsorption rate in the first 30 min and a rather slow one thereafter. This would indicate an approximately constant effect of temperature on the adsorption capacity (Fig. 10). This information is essential for practical application as mostly the textile dye effluents are discharged at relatively high temperatures (50°C–60°C) [37]. The reason for this may be that the ion-pair complexes formed between the adsorbed BCG molecules and the ZIF particles are so strong to resist against the thermal motion effect. The non-adsorbed yet molecules are enhanced by their mobility to move towards vacant sites of ZIF-11 particles where they can be adsorbed. However, it can be noticed that the efficiency removal increased from about 74% to a maximum of 88% with the increase of contact time above 30 min up to 70 min for the temperature settings investigated. Comparatively, the first 30 min of the process is more cost-effective and therefore the choice of this value is supported.

3.3. Adsorption isotherms

The well-known Langmuir, Freundlich, Temkin, and Dubinin-Radushkevich adsorption isotherms were used to study the adsorption of BCG onto ZIF-11. Table 1 summarizes the linearized and non-linearized equations of these models.

3.3.1. Langmuir isotherm model

The Langmuir adsorption isotherm is generally suitable for describing the monolayer adsorption process. The Langmuir isotherm equation includes two parameters: a constant K_L, which refers to the affinity between the adsorbate and the adsorbent, and the maximum adsorption amount Q_m. These parameters are combined in a dimensionless constant named separation factor designed by R_L and given as [38]:

$$R_L = \frac{1}{1 + K_L C_0} \tag{8}$$

with the following features:

- When $R_L > 1$, affinity is low (desorption is preferred);
- When $R_L = 1$, adsorption is regular (Henry's law);
- When $0 < R_L < 1$, affinity is high (adsorption is preferred).

3.3.2. Freundlich isotherm model

When the adsorbent surface is heterogeneous, it is likely but not proved to use the Freundlich isotherm equation. This model, also, introduces two parameters: a constant K_F and an exponent of non-linearity $1/n$, with the following features [39]:

- When $1/n = 1$, the curve is linear (Henry's law);
- When $1/n < 0.7$, the curve is pronounced.

Table 1
Langmuir, Freundlich, Temkin, and Dubinin-Radushkevich adsorption isotherm: linearized and non-linearized equations

Isotherm models	Equations	Linearized form	Plot
Langmuir	$Q_e = \frac{Q_m K_L C_e}{1 + K_L C_e}$	$\frac{1}{Q_e} = \frac{1}{K_L Q_m C_e} + \frac{1}{Q_m}$	$\frac{1}{Q_e}$ vs. $\frac{1}{C_e}$
Freundlich	$Q_e = K_F \sqrt[n]{C_e}$	$\mathrm{Ln}(Q_e) = \ln K_F + \frac{1}{n}\ln C_e$	$\ln Q_e$ vs. $\ln C_e$
Temkin	$Q_e = \frac{RT}{B}\ln(K_T C_e)$	$Q_e = \frac{RT}{B}\ln K_T + \frac{RT}{B}\ln C_e$	Q_e vs. $\ln C_e$
Dubinin-Radushkevich	$Q_e = Q_s e^{-K_{ad}\varepsilon^2}$	$\ln(Q_e) = \ln Q_s - K_{ad}\varepsilon^2$	$\ln Q_e$ vs. ε^2

3.3.3. Temkin isotherm model

The Temkin isotherm model takes into account the effects of indirect adsorbate/adsorbate interactions on the adsorption process; the decrease in heat of adsorption is linear rather than logarithmic, as implied by the Freundlich equation. The isotherm equation as well includes two parameters: the equilibrium-binding constant K_T and the Temkin constant B, which is related to the constant of heat of sorption b [40].

$$B = RTb^{-1} \tag{9}$$

3.3.4. Dubinin-Radushkevich isotherm model

The Dubinin-Radushkevich isotherm equation is, in general, widely used for homogeneous and heterogeneous surface adsorption [41]. This model contains two parameters: the activity coefficient K_{ad} useful in obtaining the mean sorption energy E and the theoretical adsorption capacity Q_s of the Dubinin-Radushkevich monolayer saturation, whereas ε is the Polanyi potential described as:

$$\varepsilon = RT\ln\left(1 + \frac{1}{C_e}\right) \tag{10}$$

The mean free energy of adsorption per molecule of adsorbate required to transfer 1 mol of BCG dye from the infinity in the solution to the surface of ZIF-11 can be calculated by Eq. (11) [42].

$$E = \frac{1}{\sqrt{2K_{ad}}} \tag{11}$$

The experimental data of BCG adsorption isotherms on ZIF-11 collected at different concentrations of 40 to 300 mg/L were fitted to these models. A non-linear method was used to estimate the parameters in the different equations by minimizing the SSE, between experimental and calculated data by means of the solver add-in program of Microsoft Excel. For linearized equations, linear regression was commonly used.

3.4. Adsorption isotherm analysis

The plots of non-linearized and linearized equations for the adsorption isotherms of Langmuir, Freundlich, Temkin, and Dubinin-Radushkevich are presented in Figs. 11 and 12. The statistical criterions associated to these models were calculated and given in Table 2, whereas the parameters of these models were found and given in Table 3.

As shown in Figs. 11 and 12, the Langmuir isotherm firstly and the Temkin isotherm secondly are well fitted for the BCG adsorption onto ZIF-11. This finding is supported by the correspondingly higher R^2 values and lower standard errors (Table 2). In addition, the isotherm parameters, namely Langmuir and Temkin constants had, respectively, lower values K_L = 0.042 L/mg and K_T = 0.074 L/mg (Table 3) showing the weak interactions between BCG and ZIF-11, whereas the low value for the separation factor (R_L = 0.37) indicated that the BCG adsorption onto

Table 2
Statistical criterions associated to Langmuir, Freundlich, Temkin, and Dubinin-Radushkevich models for the BCG adsorption onto ZIF-11

Statistics	Langmuir	Freundlich	Temkin	Dubinin-Radushkevich
SSE	137.9	1,181.1	348.9	1,365.9
RMSE	3.54	10.4	5.6	11.1
HYBRID	20.9	228.9	41.8	359.1
χ^2	1.88	20.6	3.76	32.3
R^2	0.97	0.94	0.96	0.64

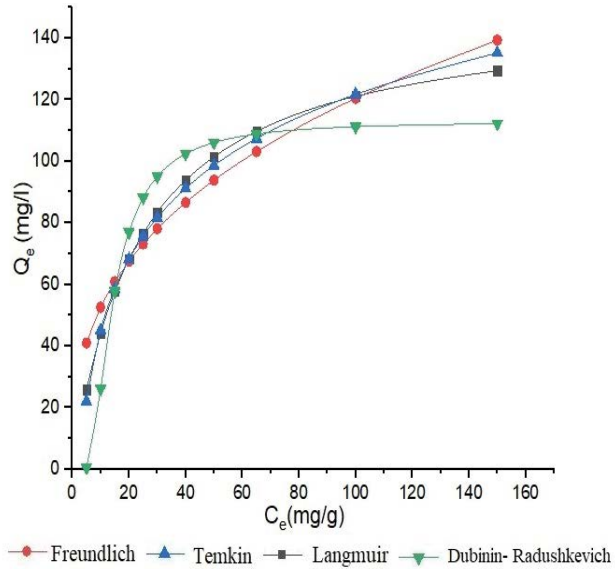

Fig. 11. Experimental isotherms and non-linear equation plots of Langmuir, Freundlich, Temkin, and Dubinin-Radushkevich isotherms for the BCG adsorption onto ZIF-11.

ZIF-11 is favorable. This is evidenced by the maximum capacity of adsorption for Langmuir isotherm determined by the non-linear method (Q_m = 150 mg/g). Therefore, the Langmuir and Temkin models can provide good interpretation for the experimental data in contrast to Freundlich and Dubinin-Radushkevich models, which showed poor fit that resulted in excessive values for statistical error functions (Table 2).

3.5. Adsorption kinetics

The pseudo-first-order (PFO), pseudo-second-order (PSO), and intraparticle diffusion (IP) models have been commonly used to represent the kinetics of adsorption [43]. The equations corresponding to these models are summarized in Table 4. In these equations, Q_e and Q_t (mg/g) are the amounts of the BCG dye adsorbed at equilibrium and at time t (min), respectively, K_1 (min^{-1}) is the rate constant for the PFO, K_2 (g/mg min) is the rate constant for the PSO. K_p (mg/g min$^{0.5}$) is the IP rate constant and C is the intercept for the IP. In this study, the kinetic parameters were assessed by fitting these models to experimental data, which were recorded for a set of BCG adsorption experiments with an

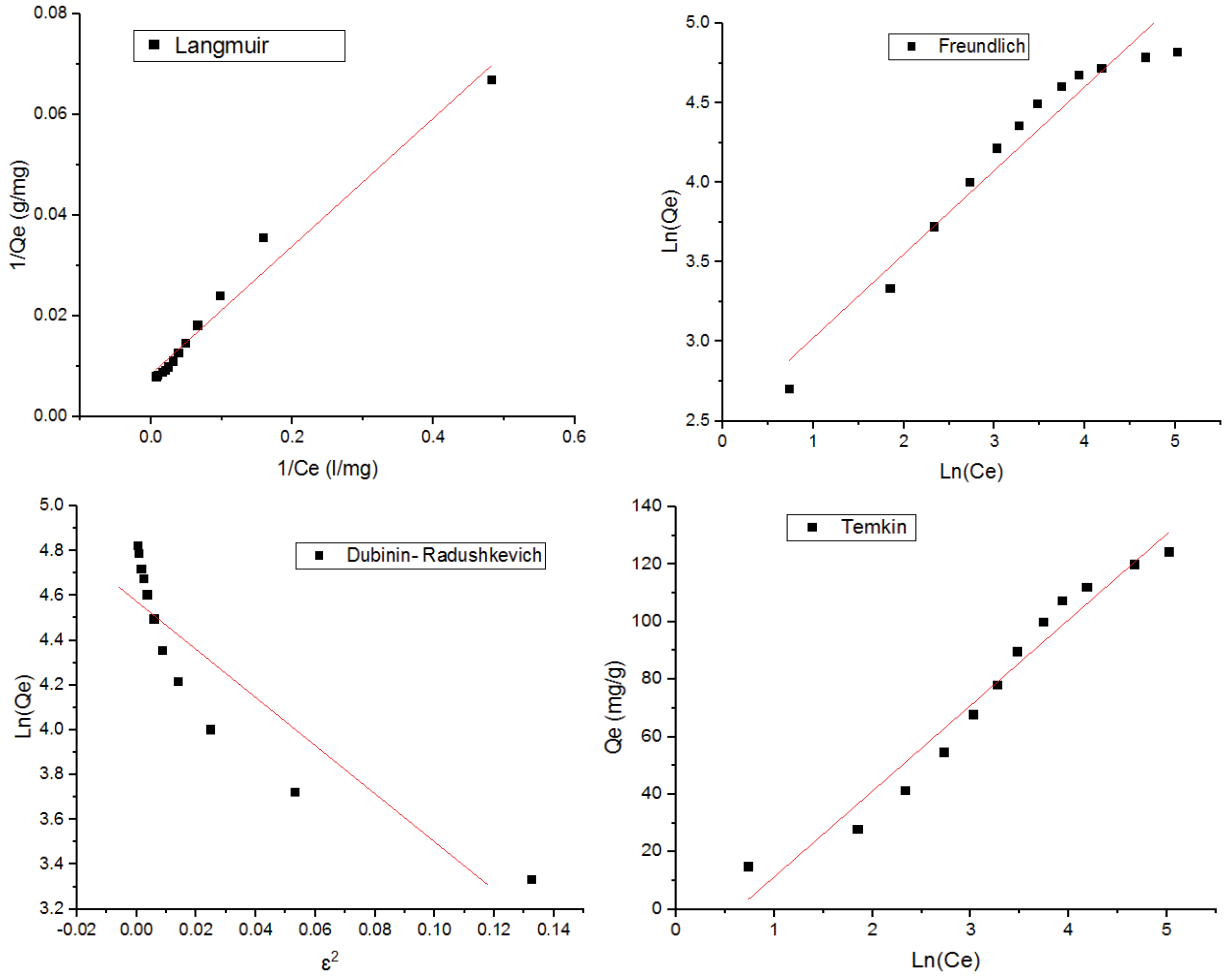

Fig. 12. Linearized equation plots of Langmuir, Freundlich, Temkin, and Dubinin-Radushkevich isotherms for the BCG adsorption onto ZIF-11.

Table 3
Langmuir, Freundlich, Temkin, and Dubinin-Radushkevich isotherms parameters for the adsorption of BCG onto ZIF-11

Langmuir		Freundlich		Temkin		Dubinin-Radushkevich	
K_L (L/mg)	0.042	K_F	22.97	K_T (L/mg)	0.39	K_{ad} (mg/kJ)	26.26
Q_m (mg/g)	150.2	n	2.78	B (J/mol)	74.49	Q_s (mg/g)	113.01
R_L	0.373					E (kJ)	0.14

Table 4
Kinetic models: linearized and non-linearized equations

Kinetic models	Equations	Plot	Linearized form	Plot
Pseudo-first-order	$Q_t = Q_e\left(1-\mathrm{Exp}\left(-k_1 t\right)\right)$	Q_t vs. t	$\ln\left(Q_e - Q_t\right) = \ln Q_e - k_1 t$	$\ln(Q_e - Q_t)$ vs. t
Pseudo-second-order	$Q_t = \dfrac{t}{\dfrac{1}{k_2 Q_e^2} + \dfrac{t}{Q_e}}$	Q_t vs. t	$\dfrac{t}{Q_t} = \dfrac{1}{k_2 Q_e^2} + \dfrac{t}{Q_e}$	t/Q_t vs. t
Intraparticle diffusion	$Q_t = K_p t^{0.5} + C$	Q_t vs. t	$Q_t = K_p t^{0.5} + C$	Q_t vs. $\sqrt{t}$

initial concentration of 200 mg/L and a contact time ranging from 0 to 70 min. The linearized equations required the common linear regression analysis, whereas the non-linear equations required a non-linear method, which minimizes the SSE between experimental and calculated data by a trial and error procedure, which is applicable to computer operation. For this purpose, the solver add-in program of Microsoft Excel was used.

The linear plots related to the PFO, PSO, and IP models are presented in Fig. 13, whereas the non-linear plots are presented in Fig. 14. The constant values deducted from these plots and the statistical criterions are reported in Table 5. The kinetic data analysis indicated that the experimental data sufficiently fitted the PFO model for the time range from 0 to 40 min (Fig. 13) and fitted well the PSO model for the entire time range (Figs. 13 and 14). The statistical analysis also showed better values for the PSO model fitting (Table 5). It has been reported that the PSO reaction kinetics provide the best correlation of the experimental data for many sorption processes, excepted those occurring onto inhomogeneous solid surfaces controlled by diffusion [44]. Indeed, more caution should be exercised in the analysis of kinetic data, especially for the systems controlled by diffusion [43]. Conveniently, the IP model fitting showed a bilinearity plot with satisfactory statistical errors (Fig. 13 and Table 5). This suggested that a part of BCG molecules instantaneously adsorbed on the ZIF-11 external surface and next, another

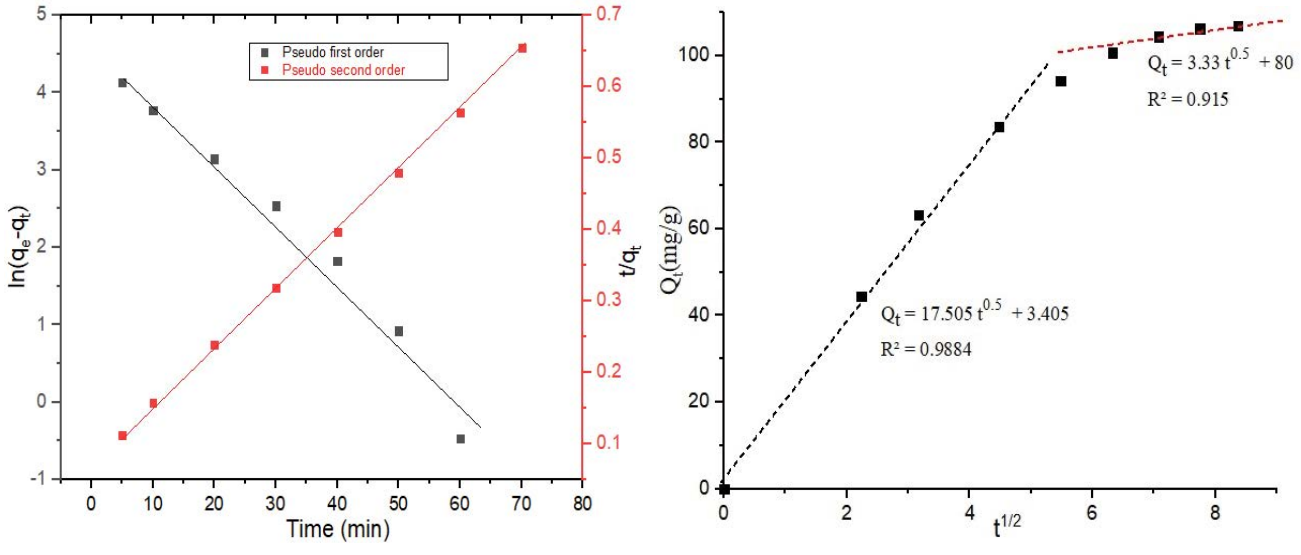

Fig. 13. Plots of fitted PFO and PSO linearized models (left) and IP linearized model (right) for the BCG adsorption onto ZIF-11.

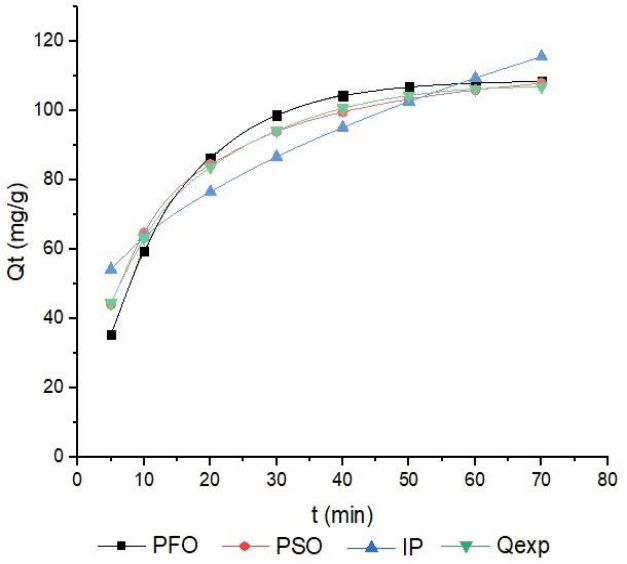

Fig. 14. Plots of the experimental data and fitted PFO, PSO, and IP non-linear models for the BCG adsorption onto ZIF-11.

part of molecules gradually diffused within their pores, where IP is controlled.

Obviously, the BCG adsorption onto ZIF-11 followed a physicochemical sorption mechanism, which was confirmed by low values of thermodynamic BCG adsorption parameters (Section 3.6).

3.6. Thermodynamic parameters

Thermodynamic parameters of adsorption provide performance estimation and prediction of the adsorption mechanism and are required for the characterization and optimization of an adsorption process [45]. The Gibb's free energy change ($\Delta G°$) is an important criterion for adsorption spontaneity. $\Delta G°$ for BCG adsorption onto ZIF-11 was determined by classical Van't Hoff equation:

$$\Delta G° = -RT\ln K_d \tag{12}$$

where K_d is the constant partition coefficient defined as [46]:

$$K_d = \frac{Q_e}{C_e} \tag{13}$$

where Q_e (mg/g) is the amount of adsorbed BCG onto ZIF-11 and C_e (mg/L) is the equilibrium BCG concentration in solution.

$\Delta G°$ is related to adsorption enthalpy change $\Delta H°$ and adsorption entropy change $\Delta S°$ by:

$$\Delta G° = \Delta H° - T\Delta S° \tag{14}$$

Considering this relation, Eq. (12) gives:

$$\ln K_d = \frac{\Delta S°}{R} - \frac{\Delta H°}{RT} \tag{15}$$

The experimental data of Q_e and C_e, which served to calculate K_d were obtained for the temperature values (298, 313, and 323 K). By plotting $\ln K_d$ vs $1/T$ (Fig. 15) the values of $\Delta H°$ and $\Delta S°$ were determined. Finally, $\Delta G°$ values were found (Table 6). The activation energy E_a and sticking probability s^* were determined from experimental measurements of the adsorption rate constant at different temperatures according to the Arrhenius equation as follows [10]:

$$s^* = (1-\theta)e^{-\frac{E_a}{RT}} \tag{16}$$

The sticking probability s^* is a function of the adsorbate/adsorbent system and θ is a parameter defined as:

$$\theta = 1 - \frac{C_e}{C_0} \tag{17}$$

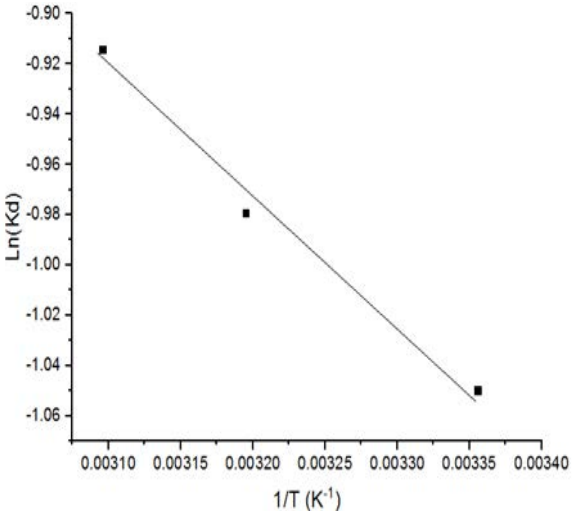

Fig. 15. $\ln K_d = f(1/T)$ plot for the BCG adsorption onto ZIF-11.

Table 5
Kinetic parameters obtained from various kinetic models for sorption of BCG

Parameters values	Rate constant	Model constant	R^2	SSE	HYBRID	RMSE	χ^2
Pseudo-first-order	K_1 = –0.079	Q_e = 109 mg/g	0.079	146.87	42.97	4.28	2.58
Pseudo-second-order	K_2 = 0.113	Q_e = 122 mg/g	0.999	6.47	1.33	0.90	0.08
Intraparticle diffusion	K_p = 10.02	C = 31.79	(0.98/0.91)	321.83	74.49	6.34	4.47

Table 6
Thermodynamic parameters and its plot error values for the adsorption of BCG onto ZIF-11

T (K)	$-\Delta G°$ (kJ/mol)	$\Delta H°$ (kJ/mol)	$\Delta S°$ (kJ/mol K)	R^2	RMSE	SSE	Hybrid
298	4.37						
313	4.77	4.27	0.03	1	0.37	0.41	0.69
323	5.10						

Eq. (16) can be written as:

$$\ln(1-\theta) = \ln s^* + \frac{E_a}{RT} \quad (18)$$

By plotting ln(1 − θ) vs 1/T for the temperature values (298, 313, and 323 K) (Fig. 16) E_a and s^* were determined.

As seen in Table 6, $\Delta G°$ values were found to be negative, indicating that the adsorption process of BCG on ZIF-11 was spontaneous and feasible, especially at high temperatures, in accordance with the decrease of the negative values of $\Delta G°$ as the temperature increased from 298 to 323 K. In this regard, the positive values of $\Delta S°$ also suggested the mobility of the BCG molecules in solution, which is indicative of an increased randomness at the solid/solution interface and a good affinity of BCG for ZIF-11. The positive values for $\Delta H°$ indicated that the adsorption process was endothermic. Indeed, as the previously adsorbed water molecules might desorb prior to the adsorption of the BCG molecules onto the ZIF-11 particles heat supply was needed [45]. The obtained positive values of E_a = {8.9; 9.4; 9.7} kJ/mol and s^* = 0.027 (Fig. 16) indicated the endothermic nature of the adsorption process on one hand and the magnitude of the probability of BCG dye to stick on the surface of ZIF-11. These values can be referred to a physicochemical adsorption process. These findings are in agreement with the reports of dye adsorption studies on different adsorbents [45].

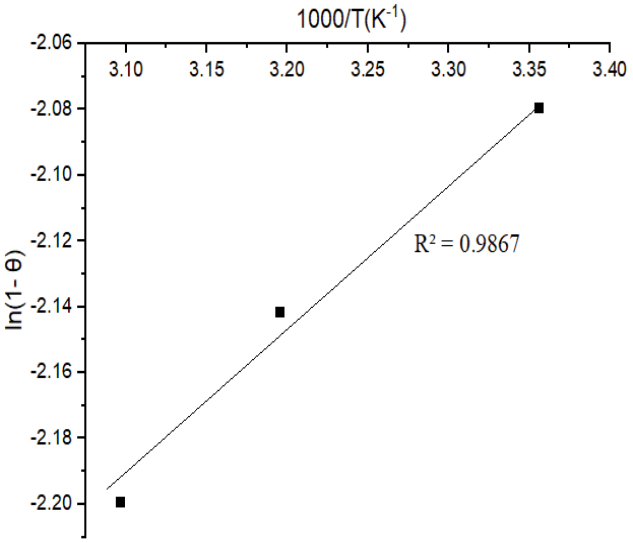

Fig. 16. Plots of ln(1 − θ) vs. 1/T for the adsorption of BCG onto ZIF-11.

3.7. Comparison of ZIF-11 performance with the other adsorbents

As shown in Table 7, the adsorption capacity for ZIF-11 is compared to other synthetic adsorbents. Considering its rapid and facile synthesis and good adsorption performance, ZIF-11 would be a promising adsorbent for the efficient removal of BCG from aqueous solutions.

Table 7
Comparison of BCG maximum adsorption capacity of ZIF-11 with some adsorbents reported in the literature

Adsorbent	Adsorption capacity (mg/g)	References
Cd(OH)2-NW-AC	108.7	[9]
Ziziphus nummularia	6.21	[10]
Cotton stalks activated carbon	222.22	[12]
Chitosan poly(methacrylate) composites	39.84	[13]
Electrospun scaffolds	2.93	[14]
ZIF-11	150.20	This work

4. Conclusion

In this study, ZIF-11 was synthesized by stirring method and successfully tested as an adsorbent for BCG. It showed particular characteristics such as porosity, morphology, high crystallinity, and thermal stability, which are the required features for the removal of dyes such as BCG from its aqueous solution. The BCG adsorption performance and efficiency were, respectively, evidenced by high adsorption capacity (Q_m = 150.20 mg/g) and reduced duration (contact time = 30 min). These settings were supported by the adsorption equilibrium and kinetics studies. The experimental adsorption data fitted well to Langmuir and Temkin isotherms and the rate was PSO: BCG molecules rapidly adsorbed on the external ZIF-11 surface and subsequently diffused within their particle pores. This mechanism consisted of electrostatic interactions between Zn^{2+} ions of ZIF-11 and SO^{3-} ions of BCG at the pH range (from 2.0 to 8.0). Consequently, the BCG adsorption onto ZIF-11 was a spontaneous physicochemical process as supported by the calculated thermodynamic parameters. Thus, it can be concluded that ZIF-11 is an effective adsorbent for the removal of BCG dyes.

Declaration of competing interest

We declare that we have no financial and personal relationships with other people or organizations that can inappropriately influence our work; there is no professional or other personal interest of any nature or kind in any product, service, and/or company that could be construed as influencing the position presented in, or the review of, the manuscript entitled.

Acknowledgments

The authors express their appreciation to the Algerian Directorate General for Scientific Research and Technological Development (DGRSDT) for the financial support of this work.

References

[1] J. Malina, A. Rađenović, Kinetic aspects of methylene blue adsorption on blast furnace sludge, Chem. Biochem. Eng. Q., 28 (2014) 491–498.
[2] T. Yin, Y. Wu, P. Shi, A.M. Li, B. Xu, W.H. Chu, Y. Pan, Anion-exchange resin adsorption followed by electrolysis: a new disinfection approach to control halogenated disinfection byproducts in drinking water, Water Res., 168 (2020) 115144, doi: 10.1016/j.watres.2019.115144.
[3] C. Wolf, A. Pavese, U. von Gunten, T. Kohn, Proxies to monitor the inactivation of viruses by ozone in surface water and wastewater effluent, Water Res., 166 (2019) 115088, doi: 10.1016/j.watres.2019.115088.
[4] C. Benally, S.A. Messele, M.G. Gamal El-Din, Adsorption of organic matter in oil sands process water (OSPW) by carbon xerogel, Water Res., 145 (2019) 402–411.
[5] Y.F. Wei, H. Liu, C.B. Liu, S.L. Luo, Y.T. Liu, X.W. Yu, J.H. Ma, K. Yin, H.P. Feng, Fast and efficient removal of As(III) from water by $CuFe_2O_4$ with peroxymonosulfate: effects of oxidation and adsorption, Water Res., 150 (2019) 182–190.
[6] C. Patra, T. Shahnaz, S. Subbiah, S. Narayanasamy, Comparative assessment of raw and acid-activated preparations of novel Pongamia pinnata shells for adsorption of hexavalent chromium from simulated wastewater, Environ. Sci. Pollut. Res., 27 (2020) 14836–14851.
[7] T. Shahnaz, C. Patra, V. Sharma, N. Selvaraju, A comparative study of raw, acid-modified and EDTA-complexed Acacia auriculiformis biomass for the removal of hexavalent chromium, Chem. Ecol., 36 (2020) 360–381.
[8] R.W. Sabnis, Handbook of Acid-Base Indicators, Taylor & Francis Group, LLC., CRC Press (Taylor & Francis Group) Boca Raton, London, New York, 2008, pp. 43–44, ISBN 978-0-8493-8218-5
[9] M. Ghaedi, H. Khajesharifi, A.H. Yadkuri, M. Roosta, R. Sahraei, A. Daneshfar, Cadmium hydroxide nanowire loaded on activated carbon as efficient adsorbent for removal of Bromocresol Green, Spectrochim. Acta, Part A, 86 (2012) 62–68.
[10] A. Shokrollahi, A. Alizadeh, Z. Malekhosseini, M. Ranjbar, Removal of Bromocresol Green from aqueous solution via adsorption on *Ziziphus nummularia* as a new, natural, and low-cost adsorbent: kinetic and thermodynamic study of removal process, J. Chem. Eng. Data, 56 (2011) 3738–3746.
[11] Y.J. Lu, B. Wei, Y. Wang, J.Z. Li, Studies on the removal of bromocresol green from water by solvent sublation, Sep. Sci. Technol., 42 (2007) 1901–1911.
[12] M. Özdemir, Ö. Durmuş, Ö. Şahin, C. Saka, Removal of methylene blue, methyl violet, rhodamine B, alizarin red, and bromocresol green dyes from aqueous solutions on activated cotton stalks, Desal. Water Treat., 57 (2015) 18038–18048.
[13] D. Liu, J. Yuan, J.W. Li, G.H. Zhang, Preparation of chitosan poly(methacrylate) composites for adsorption of Bromocresol Green, ACS Omega, 4 (2019) 12680–12686.
[14] A.I. Sokolova, E.R. Pavlova, D.V. Bagrov, D.V. Klinov, K.V. Shaitan, Dye adsorption onto electrospun films made of polylactic acid and gelatin, Mol. Cryst. Liq. Cryst., 669 (2018) 126–133.
[15] V.K.-M. Au, Recent advances in the use of metal-organic frameworks for dye adsorption, Front. Chem., 28 (2020) 1–7, doi: 10.3389/fchem.2020.00708.
[16] X.C. Xie, X.J. Huang, W.X. Lin, Y.F. Chen, X.R. Lang, Y.J. Wang, L.H. Gao, H.L. Zhu, J.J. Chen, Selective adsorption of cationic dyes for stable metal–organic framework ZJU-48, ACS Omega, 5 (2020) 13595–13600.
[17] J.-P. Zhang, Y.-B. Zhang, J.-B. Lin, X.-M. Chen, Metal azolate frameworks: from crystal engineering to functional materials, Chem. Rev., 112 (2012) 1001–1033.
[18] X.-C. Huang, Y.-Y. Lin, J.-P. Zhang, X.-M. Chen, Ligand-directed strategy for zeolite-type metal–organic frameworks: zinc(II) imidazolates with unusual zeolitic topologies, Angew. Chem. Int. Ed., 45 (2006) 1557–1559.
[19] K.S. Park, N. Zheng, A.P. Côté, J.Y. Choi, R. Huang, F.J. Uribe-Romo, H.K. Chae, M. O'Keeffe, O.M. Yaghi, Exceptional chemical and thermal stability of zeolitic imidazolate frameworks, Proc. National Acad. Sci., 103 (2006) 10186–10191.
[20] X.Y. Li, X.Y. Gao, L.H. Ai, J. Jiang, Mechanistic insight into the interaction and adsorption of Cr(VI) with zeolitic imidazolate framework-67 microcrystals from aqueous solution, Chem. Eng. J., 274 (2015) 238–246.
[21] Y. Pan, Z. Li, Z. Zhang, X.-S. Tong, H. Li, C.-Z. Jia, B. Liu, C.-Y. Sun, L.-Y. Yang, G.-J. Chen, D.-Y. Ma, Adsorptive removal of phenol from aqueous solution with zeolitic imidazolate framework-67, J. Environ. Manage., 169 (2016) 167–173.
[22] K.-Y.A. Lin, H.-A. Chang, Ultra-high adsorption capacity of zeolitic imidazole framework-67 (ZIF-67) for removal of malachite green from water, Chemosphere, 139 (2015) 624–631.
[23] Y. Li, K. Zhou, M. He, J.F. Yao, Synthesis of ZIF-8 and ZIF-67 using mixed-base and their dye adsorption, Microporous Mesoporous Mater., 234 (2016) 287–292.
[24] X.-D. Du, C.-C. Wang, J.-G. Liu, X.-D. Zhao, J. Zhong, Y.-X. Li, J. Li, P. Wang, Extensive and selective adsorption of ZIF-67 towards organic dyes: performance and mechanism, J. Colloid Interface Sci., 506 (2017) 437–441.
[25] Y. Feng, Y. Li, M.Y. Xu, S.C. Liu, J.F. Yao, Fast adsorption of methyl blue on zeolitic imidazolate framework-8 and its adsorption mechanism, RSC Adv., 6 (2016) 109608–109612.
[26] L.-B. Sun, J.-R. Li, J.H. Park, H.-C. Zhou, Cooperative template-directed assembly of mesoporous metal–organic frameworks, J. Am. Chem. Soc., 134 (2011) 126–129.
[27] H.P. Hu, S.Q. Liu, C.Y. Chen, J.P. Wang, Y. Zou, L.H. Lin, S.Z. Yao, Two novel zeolitic imidazolate frameworks (ZIFs) as sorbents for solid-phase extraction (SPE) of polycyclic aromatic hydrocarbons (PAHs) in environmental water samples, Analyst, 139 (2014) 5818–5826.
[28] E.M. Forman, B.R. Pimentel, K.J. Ziegler, R.P. Lively, S. Vasenkov, Microscopic diffusion of pure and mixed methane and carbon dioxide in ZIF-11 by high field diffusion NMR, Microporous Mesoporous Mater., 248 (2017) 158–163.
[29] M. He, J.F. Yao, Q. Liu, Z.X. Zhong, H.T. Wang, Toluene-assisted synthesis of RHO-type zeolitic imidazolate frameworks: synthesis and formation mechanism of ZIF-11 and ZIF-12, Dalton Trans., 42 (2013) 16608–16613.
[30] T. Koley, P. Bandyopadhyay, A.K. Mohanty, S. Banerjee, Synthesis and characterization of new aromatic poly(ether imide)s and their gas transport properties, Eur. Polym. J., 49 (2013) 4212–4223.
[31] M. Şafak Boroğlu, Structural characterization and gas permeation properties of polyetherimide (PEI)/zeolitic imidazolate (ZIF-11) mixed matrix membranes, J. Turkish Chem. Soc., Sect. A: Chem., 3 (2016) 183–206.
[32] A. Madanagopal, S. Periandy, P. Gayathri, S. Ramalingam, S. Xavier, V.K. Ivanov, Spectroscopic and computational investigation of the structure and pharmacological activity of 1-benzylimidazole, J. Taibah Univ. Sci., 11 (2017) 975–996.
[33] J.J.M. Órfão, A.I.M. Silva, J.C.V. Pereira, S.A. Barata, I.M. Fonseca, P.C.C. Faria, M.F.R. Pereira, Adsorption of a

reactive dye on chemically modified activated carbons—influence of pH, J. Colloid Interface Sci., 296 (2006) 480–489.
[34] A.B. Yumru, M.S. Boroglu, I. Boz, ZIF-11/Matrimid® mixed matrix membranes for efficient CO_2, CH_4 and H_2 separations, Greenhouse Gases Sci. Technol., 8 (2018) 529–541.
[35] Y.-F. Lin, K.-W. Huang, B.-T. Ko, K.-Y.A. Lin, Bifunctional ZIF-78 heterogeneous catalyst with dual Lewis acidic and basic sites for carbon dioxide fixation via cyclic carbonate synthesis, J. CO_2 Util., 22 (2017) 178–183.
[36] M.K. Dahri, L.B.L. Lim, C.C. Mei, Cempedak durian as a potential biosorbent for the removal of Brilliant Green dye from aqueous solution: equilibrium, thermodynamics and kinetics studies, Environ. Monit. Assess., 187 (2015) 546.
[37] Z. Aksu, Application of biosorption for the removal of organic pollutants: a review, Process Biochem., 40 (2005) 997–1026.
[38] K.R. Hall, L.C. Eagleton, A. Acrivos, T. Vermeulen, Pore- and solid diffusion-kinetics in fixed-bed adsorption under constant-pattern conditions, Ind. Eng. Chem. Fundam., 5 (1966) 212–223.
[39] B. Van der Bruggen, Freundlich Isotherm, E. Drioli, L. Giorno, Eds., Encyclopedia of Membranes, Springer, Berlin, Heidelberg, 2014, pp. 1–2.
[40] M.I. Temkin, V. Pyzhev, Kinetics of ammonia synthesis on promoted iron catalysts, Acta Physicochim. URSS, 12 (1940) 217–222.
[41] K. Vijayaraghavan, T.V.N. Padmesh, K. Palanivelu, M. Velan, Biosorption of nickel(II) ions onto *Sargassum wightii*: application of two-parameter and three-parameter isotherm models, J. Hazard. Mater., 133 (2006) 304–308.
[42] J.P. Hobson, Physical adsorption isotherms extending from ultra-high vacuum to vapor pressure, J. Phys. Chem., 73 (1969) 2720–2727.
[43] J.-P. Simonin, On the comparison of pseudo-first order and pseudo-second order rate laws in the modeling of adsorption kinetics, Chem. Eng. J., 300 (2016) 254–263.
[44] Y.S. Ho, G. McKay, Pseudo-second order model for sorption processes, Process Biochem., 34 (1999) 451–465.
[45] P. Saha, S. Chowdhury, Insight into Adsorption Thermodynamics, T. Mizutani, Ed., Thermodynamics, IntechOpen, 16 (2011) 349–364, doi: 10.5772/13474.
[46] K.M. Krupka, D.I. Kaplan, G.W. Shas, R.J. Serne, V. Mattigod, Understanding Variation in Partition Coefficient, Kd, Values, Volume 1: The Kd Model, Methods of Measurement, and Application of Chemical Reaction Codes, Office of Air and Radiation, Office of Solid Waste and Emergency Response, U.S. Environmental Protection Agency, Washington, D.C., 1999, p. 63.